Evaluation of F-537-Tetrazine in a model for brain pretargeting imaging: comparison to N-(3-[18F] fluoro-5-(1,2,4,5-tetrazin-3-yl)benzyl)propan-1-amine

Shalgunov, V.; Broek, S.L. van den; Andersen, I.V.; Raval, N.R.; Schäfer, G.; Barz, M.; ... ; Battisti, U.M.

Nuclear Medicine and Biology 128-129 (2024) 108877

Contents lists available at ScienceDirect

Nuclear Medicine and Biology

journal homepage: www.elsevier.com/locate/nucmedbio

Evaluation of F-537-Tetrazine in a model for brain pretargeting imaging. Comparison to N-(3-[^{18}F] fluoro-5-(1,2,4,5-tetrazin-3-yl)benzyl) propan-1-amine☆

Vladimir Shalgunov [a], Sara Lopes van den Broek [a], Ida Vang Andersen [a], Nakul R. Raval [b], Gabriela Schäfer [c], Matthias Barz [c], Matthias M. Herth [a,d,*], Umberto M. Battisti [a,**]

[a] Department of Drug Design and Pharmacology, Faculty of Health and Medical Sciences, University of Copenhagen, Universitetsparken 2, 2100 Copenhagen, Denmark
[b] Neurobiology Research Unit and Center for Integrated Molecular Brain Imaging, Rigshospitalet Copenhagen University Hospital, Blegdamsvej 9, DK-2100 Copenhagen, Denmark
[c] Leiden Academic Centre for Drug Research, Leiden University, Einsteinweg 55, 2333CC Leiden, the Netherlands
[d] Department of Clinical Physiology, Nuclear Medicine & PET, Rigshospitalet Copenhagen University Hospital, Blegdamsvej 9, 2100 Copenhagen, Denmark

ARTICLE INFO

Keywords:
Imaging
Pretargeting
Tetrazine ligation
Blood-brain-barrier

ABSTRACT

Brain pretargeted nuclear imaging for the diagnosis of various neurodegenerative diseases is a quickly developing field. The tetrazine ligation is currently the most explored approach to achieve this goal due to its remarkable properties. In this work, we evaluated the performance of F-537-Tetrazine, previously developed by Biogen, and N-(3-[^{18}F]fluoro-5-(1,2,4,5-tetrazin-3-yl)benzyl)propan-1-amine, previously developed in our group, thereby allowing for the direct comparison of these two imaging probes. The evaluation included synthesis, radiolabeling and a comparison of the physicochemical properties of the compounds. Furthermore, their performance was evaluated by in vitro and in vivo pretargeting models. This study indicated that N-(3-[^{18}F] fluoro-5-(1,2,4,5-tetrazin-3-yl)benzyl)propan-1-amine might be more suited for brain pretargeted imaging.

1. Introduction

In the last decades, pretargeted imaging emerged as a new attractive imaging technique especially in positron emission tomography (PET) [1–3]. Pretargeting allows for the usage of macromolecules, usually antibodies (Abs), enhancing imaging contrast and reducing patient radiation burden [1,2]. This can be achieved by administration of a tagged non-radioactive Ab days before the radioactive imaging agent is injected. The latter can react bioorthogonally with the tag of the Ab, generating a radiolabeled Ab in vivo for selective target imaging. Several bioorthogonal reactions have been discovered, of which the tetrazine ligation between a trans-cyclooctene (TCO) and a tetrazine (Tz) stands out as the most promising reaction for pretargeting due to its high selectivity and fast reaction kinetics. [1,2,4,5]. The tetrazine ligation is initiated via an inverse-electron-demand Diels–Alder (IEDDA) reaction and undergoes subsequently a retro-Diels-Alder reaction, with the elimination of nitrogen gas [6]. As such, the tetrazine ligation is irreversible and yields in a stable product [6]. From the two reaction partners, TCOs are usually conjugated to the pretargeting vector such as Abs, and tetrazines are used as imaging probes [7,8].

The first Tzs developed for this purpose bore a chelating moiety such as NOTA, DOTA and were labeled exclusively with radiometals [9–13]. This approach was mainly selected due to the ease of chelation chemistry and the relative instability of tetrazines which prohibited the use of more complex reactions [14]. However, this strategy limited the use of pretargeted imaging mainly to extracellular targets in peripheral tissues due to the size and the polarity of the resulting probe [15,16]. Recently, new methodologies were reported to label highly reactive tetrazines

☆ This is a free access article and can be viewed on the journal's Web site (www.nucmedbio.com). Complimentary access to this article is available until the next issue publishes online.

* Correspondence to: M. M. Herth, Department of Clinical Physiology, Nuclear Medicine & PET, Rigshospitalet Copenhagen University Hospital, Blegdamsvej 9, 2100 Copenhagen, Denmark.

** Correspondence to: U. M. Battisti, Department of Drug Design and Pharmacology, Faculty of Health and Medical Sciences, University of Copenhagen, Universitetsparken 2, 2100 Copenhagen, Denmark.

E-mail addresses: matthias.herth@sund.ku.dk (M.M. Herth), umberto.battisti@sund.ku.dk (U.M. Battisti).

https://doi.org/10.1016/j.nucmedbio.2024.108877
Received 15 October 2023; Received in revised form 5 January 2024; Accepted 5 January 2024
Available online 11 January 2024

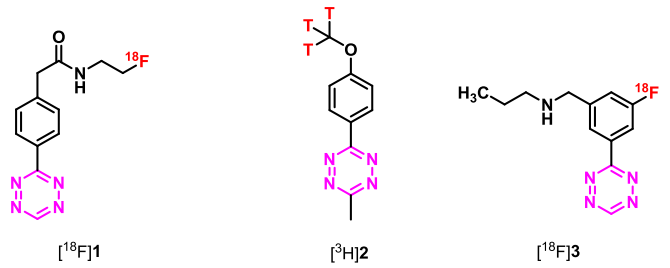

Fig. 1. Chemical structures of tetrazines developed for brain pretargeted imaging [29,30,34].

with different covalently bound radionuclides [17–21]. In particular, fluorine-18 (^{18}F) was featured in several radiolabeling strategies due to its ideal imaging properties [22–28]. In the last few years, several groups and companies developed pretargeting strategies for CNS applications. Biogen reported the successful development of an ^{18}F-labeled Tz, F-537-Tz (Fig. 1, [^{18}F]**1**) for the imaging of antisense oligonucleotides [29]. More recently, Roche tried a similar approach exploiting a TCO-conjugated brain shuttle Ab and a tritiated Tz (Fig. 1, [^{3}H]**2**) [30]. This strategy proved unsuccessful in vivo, most likely due to the low reactivity of the methylTz compound [26,29]. Our group has recently developed robust methods to radiolabel highly reactive Tzs with fluorine-18 leading to the development of a series of [^{18}F]Tzs designed for pretargeting beyond the BBB [31–34]. The best compound, tetrazine [^{18}F]**3** (Fig. 1), demonstrated a good in vitro and in vivo profile emerging as a possible candidate for future experiments [34]. In this work, we evaluated tetrazine [^{18}F]**1** with our experimental workflow and compared its in vitro and in vivo performance to our in-house developed tetrazine [^{18}F]**3**.

2. Material and methods

2.1. General

All reagents and solvents were purchased from commercial suppliers and used without further purification. Anhydrous tetrahydrofuran (THF) was obtained from an SG water solvent purification system (Pure Process Technology). Reactions requiring anhydrous conditions were carried out under an inert atmosphere (nitrogen or argon) and using oven-dried glassware (152 °C). Other solvents were analytical or HPLC grade and were used as received. NMR spectra were acquired on a 600 MHz Bruker Avance III HD (600 MHz for ^{1}H and 151 MHz for ^{13}C), a 400 MHz Bruker Avance UltraShield (400 MHz for ^{1}H, 376 MHz for ^{19}F and 101 MHz for ^{13}C), using $CDCl_3$, MeOD or DMSO-d_6 as deuterated solvent and with the residual solvent as the internal reference. Coupling constants (J values) are given in Hertz (Hz). Multiplicities of ^{1}H NMR signals are reported as follows: s, singlet; d, doublet; dd, doublet of doublets; ddd, doublet of doublets of doublets; dt, doublet of triplets; t, triplet; q, quartet; m, multiplet; br, broad signal. NMR spectra of all compounds are reprocessed in MestReNova software. Analytical HPLC method: Thermo Fisher UltiMate 3000 with a C-18 column (Luna 5 μm C18(2) 100 Å, 150 mm × 4.6 mm). Eluents: A, H_2O with 0.1 % TFA; B, CH_3CN with 0.1 % TFA. Gradient from 100 % A to 100 % B over 12 min, back to 100 % A over 3 min, flow rate 2 mL/min. Detection by UV absorption at λ = 254 nm on a UVD 170 U detector. Thin-layer chromatography (TLC) was carried out on silica gel 60 F_{254} plates from Merck (Germany). Preparative HPLC was carried out on an UltiMate HPLC system (Thermo Scientific) consisting of an LPG-3200BX pump (10 mL/min), a Rheodyne 9725i injector, a 10 mL loop, a MWD-3000SD detector (254 nm), and an AFC-3000SD automated fraction collector, using a Gemini-NX C18 column (21.2 × 250 mm, 5 μm, 110 Å) (Phenomenex) equipped with a guard. Purifications were performed using linear gradients of 0.1 % TFA in MilliQ-H_2O (A) and 0.1 % TFA, 10 % MilliQ-H_2O in CH_3CN (B). Data was acquired and processed using Chromeleon Software v. 6.80. Semi-preparative HPLC was performed on the same system using a Luna 5 μ C18 column (250 × 10 mm) with a flow rate of 3 mL/min. Automated Flash Column Chromatography was performed on a CombiFlash NextGen 300+ system supplied by TeleDyne ISCO, equipped with RediSep silica packed columns. Microwave-assisted synthesis was carried out in a Biotage Initiator apparatus operating in single mode (Biotage AB, Uppsala, Sweden). Mass spectra analysis was completed using MS-Acquity-A: Waters Acquity UPLC with QDa-detector.

Radiochemistry was performed at Department of Clinical Physiology, Nuclear Medicine & PET, Rigshospitalet, Denmark. [^{18}F]Fluoride was produced via the (p,n)-reaction in a cyclotron (60 μA CTI Siemens or 40 μA Scanditronix) by irradiating [^{18}O]H_2O with a 11 MeV (CTI siemens) or 16 MeV (Scanditronix) proton beam. Automated syntheses were performed on a Scansys Laboratorieteknik synthesis module housed in a hot cell. Analytical HPLC was performed on a Dionex system connected to a P680A pump, a UVD 170 U detector and a Scansys radiodetector. Semi-preparative HPLC was performed on the built-in HPLC system in the synthesis module and the flow rate was set to 4 mL/min at all times.

Radiochemical conversion (RCC) of all radiolabeled compounds was determined by analyzing an aliquot labeling of the reaction mixture by radio-HPLC. The products were characterized by comparing the radio-HPLC trace of the reaction mixtures with the HPLC UV traces of the authentic ^{19}F-reference samples, respectively. The radiochemical yield (RCY) was determined using the activity of [^{18}F]fluoride received from the cyclotron at the beginning of the synthesis and that of the formulated product at the end of the synthesis, the decomposition was corrected and have been decay corrected (d.c.). The molar activity (A_m) was determined by integrating the area of the UV absorbance peak corresponding to the radiolabeled product on the HPLC chromatogram. This area was converted into a molar mass by comparison with an average of integrated areas (triplet) of a known concentration for the corresponding reference compounds [35]. The values for radiochemical yield (RCY), radiochemical purity (RCP) and molar activity (A_m) are given as mean values. This applies for all radiolabeled compounds described below.

2.2. Synthesis of precursor for [^{18}F] F-537-Tz (5)

2.2.1. Synthesis of 2-(4-(1,2,4,5-tetrazin-3-yl)phenyl)acetic acid (4)

The compound was synthesized as previously reported [36]. 2-(4-Cyanophenyl)acetic acid (0.96 g, 6.00 mmol), CH_2Cl_2 (0.38 mL, 6.00 mmol), sulfur (0.38 g, 1.5 mmol), and ethanol (6.0 mL) were mixed together in a microwave reaction vial. Hydrazine monohydrate (2.34 mL, 48.00 mmol) was added dropwise while stirring. The vessel was sealed, and the reaction mixture was heated to 50 °C for 24 h. The reaction was diluted with 6 mL of CH_2Cl_2, and sodium nitrite (4.14 g, 60.00 mmol) in 40 mL of H_2O was added dropwise to the mixture under cooling. Excess acetic acid (21 mL) was then added slowly, during which the solution turned bright red in color. The reaction mixture was extracted with CH_2Cl_2 (3 × 40 mL). The organic phase was dried over $MgSO_4$ and concentrated under reduced pressure. The resulting residue was purified using flash chromatography (CH_2Cl_2/MeOH 98/2) to give 0.36 g (28 %) of the desired product as a pink solid. R_f = 0.19 (CH_2Cl_2/MeOH 95/5); ^{1}H NMR (400 MHz, MeOD) δ 10.33 (s, 1H), 8.56 (d, J = 8.4 Hz, 2H), 7.59 (d, J = 8.3 Hz, 2H), 3.78 (s, 2H); ^{13}C NMR (101 MHz, MeOD) δ 173.27, 166.24, 157.83, 140.15, 130.69, 130.13, 127.78, 40.39.

2.2.2. Synthesis of 2,5-dioxopyrrolidin-1-yl 2-(4-(1,2,4,5-tetrazin-3-yl) phenyl)acetate (5)

To a solution of 2-(4-(1,2,4,5-tetrazin-3-yl)phenyl)acetic acid (0.10 g and 0.46 mmol) in anhydrous THF (5 mL) was added N-hydroxysuccinimide (0.057 g and 0.48 mmol) and DCC (0.096 g and 0.46 mmol). The reaction was stirred at room temperature overnight. The reaction was diluted with 20 mL of CH_2Cl_2 and washed with water (2 ×

20 mL) and brine (2 × 20 mL). The organic phase was dried over $MgSO_4$ and concentrated under reduced pressure. The crude was dissolved in cold CH_3CN, filtered, and concentrated to give 0.12 g, (69 %) of the desired product as a red solid. $R_f = 0.38$ (CH_2Cl_2/MeOH 99/1); ^{1}H NMR (400 MHz, $CDCl_3$) δ 10.23 (s, 1H), 8.68–8.62 (m, 2H), 7.61 (d, $J = 8.2$ Hz, 2H), 4.07 (s, 2H), 2.86 (s, 4H); ^{13}C NMR (101 MHz, $CDCl_3$) δ 168.96, 166.32, 166.25, 158.02, 136.87, 131.39, 130.55, 128.95, 37.80, 25.75.

2.3. Synthesis of F-537-Tz (1)

To a solution of 2,5-dioxopyrrolidin-1-yl 2-(4-(1,2,4,5-tetrazin-3-yl) phenyl)acetate (0.05 g, 0.023 mmol) in anhydrous THF (5 mL) was added triethylamine (0.1 mL, 0.69 mmol) and 2-fluoroethylamine hydrochloride (0.045 g, 0.46 mmol). The reaction was stirred at room temperature for 6 h. The mixture was then diluted with 20 mL of CH_2Cl_2 and washed with water (2 × 20 mL) and brine (2 × 20 mL). The organic phase was dried over $MgSO_4$ and concentrated under reduced pressure to give 0.04 g (78 %) of the desired product as a red solid. $R_f = 0.22$ (n-Heptane/EtOAc 40/60); ^{1}H NMR (400 MHz, DMSO-d_6) δ 10.58 (s, 1H), 8.48–8.40 (m, 3H), 7.57 (d, $J = 8.2$ Hz, 2H), 4.51 (t, $J = 5.0$ Hz, 1H), 4.39 (t, $J = 5.0$ Hz, 1H), 3.62 (s, 2H), 3.43 (q, $J = 5.3$ Hz, 1H), 3.36 (q, $J = 5.2$ Hz, 1H); ^{13}C NMR (101 MHz, DMSO-d_6) δ 170.27, 165.92, 158.54, 142.02, 130.61, 130.53, 128.15, 82.90 (d, $J = 165.1$ Hz), 42.56, 40.57 (d, $J = 21.2$ Hz).

2.4. Synthesis of precursor for [^{18}F]3 (14)

2.4.1. Synthesis of 3-(bromomethyl)-5-iodobenzonitrile (6)

To a solution of 3-iodo-5-methylbenzonitrile (2.50 g, 10.28 mmol) and N-bromosuccinimide (2.28 g, 12.86 mmol) in $CHCl_3$ (40 mL) was added AIBN (0.67 g, 4.11 mmol). The reaction was refluxed for 24 h. The solvent was removed under vacuum and the crude purified by flash chromatography (n-Heptane/EtOAc 95/5) to give 1.61 g (49 %) of a white solid. $R_f = 0.28$ (n-Heptane/EtOAc 95/5); ^{1}H NMR (400 MHz, $CDCl_3$) δ 7.96 (d, $J = 1.6$ Hz, 1H), 7.89 (d, $J = 1.6$ Hz, 1H), 7.64 (t, $J = 1.6$ Hz, 1H), 4.38 (s, 2H) ^{13}C NMR (101 MHz, $CDCl_3$) δ 142.20, 140.90, 140.12, 131.67, 116.55, 114.56, 94.05, 29.90.

2.4.2. Synthesis of 3-((Propylamino)methyl)-5-iodobenzonitrile hydrochloride (8)

To a solution of the 3-(bromomethyl)-5-iodobenzonitrile (0.7 g, 2.17 mmol) in THF (20 mL) and was added propylamine (2.1 mL, 24.84 mmol). The reaction was stirred at room temperature for 5 h. The solution was concentrated and taken up with water (20 mL) and the resulting solution was extracted with CH_2Cl_2 (2 × 20 mL), washed with brine (2 × 20 mL), dried with $MgSO_4$ and filtered before concentrating under reduced pressure to afford the free amine as a yellow oil. The compound was resolubilized in Et_2O and HCl in Et_2O was added. The solid obtained was filtered and crystallized from MeOH/Et_2O to give 0.48 g (66 %) 3-((propylamino)methyl)-5-iodobenzonitrile hydrochloride as a white solid. ^{1}H NMR (600 MHz, DMSO-d_6) δ 9.39 (s, 2H), 8.33 (t, $J = 1.6$ Hz, 1H), 8.31 (t, $J = 1.6$ Hz, 1H), 8.10 (t, $J = 1.5$ Hz, 1H), 4.14 (t, $J = 5.7$ Hz, 2H), 2.89–2.76 (m, 2H), 1.73–1.59 (m, 2H), 0.91 (t, $J = 7.4$ Hz, 3H); ^{13}C NMR (151 MHz, DMSO-d_6) δ 144.01, 140.66, 135.94, 133.73, 117.47, 113.49, 95.80, 48.77, 40.55, 19.40, 11.45.

2.4.3. Synthesis of tert-butyl (3-cyano-5-iodobenzyl)(propyl)carbamate (10)

3-Iodo-5-((propylamino)methyl)benzonitrile hydrochloride (0.47 g, 1.40 mmol) and triethylamine (0.58 mL, 4.19 mmol) were dissolved in anhydrous CH_2Cl_2 (30 mL) at 0 °C. To this stirred solution was added di-tert-butyl dicarbonate (0.32 g, 1.46 mmol), and the reaction allowed to warm to room temperature and stirred for 12 h. The reaction mixture was evaporated under reduced pressure, and the residue was re-dissolved in diethyl ether (40 mL), which was washed successively with 0.5 M aq. HCl (2 × 15 mL), saturated $NaHCO_3$ (2 × 15 mL) and brine (15 mL). The organic layer was dried over anhydrous $MgSO_4$, filtered and evaporated under reduced pressure to give a white solid. The residue was purified by flash chromatography (n-Heptane/EtOAc 85/15) to afford 0.55 g (98 %) of the desired compound as a colorless oil (mixture of rotamers). $R_f = 0.55$ (n-Heptane/EtOAc 80/20); ^{1}H NMR (400 MHz, $CDCl_3$) δ 7.80 (s, 1H), 7.76 (s, 1H), 7.43 (s, 1H), 4.34 (s, 2H), 3.09 (s, 2H), 1.53–1.27 (m, 11H), 0.82 (t, $J = 7.4$ Hz, 3H); ^{13}C NMR (101 MHz, $CDCl_3$) δ 155.91, 142.49, 140.63, 138.93, 129.83, 117.01, 114.15, 93.99, 80.25, 49.05, 28.33, 21.45, 11.19.

2.4.4. Synthesis of tert-butyl (3-iodo-5-(1,2,4,5-tetrazin-3-yl)benzyl)(propyl)carbamate (12)

The compound was synthesized as previously reported [36]. *Tert*-butyl 3-cyano-5-iodobenzyl(propyl)carbamate (0.55 g, 1.37 mmol), CH_2Cl_2 (0.09 mL, 1.37 mmol), sulfur (0.09 g, 0.34 mmol), and ethanol (4.0 mL) were mixed in a microwave reaction vial. Hydrazine monohydrate (0.5 mL, 10.98 mmol) was added dropwise while stirring. The vessel was sealed, and the reaction mixture was heated to 50 °C for 24 h. The reaction was diluted with 3 mL of CH_2Cl_2, and sodium nitrite (0.95 g, 13.72 mmol) in 10 mL of H_2O was added dropwise to the mixture under cooling. Excess acetic acid (7 mL) was then added slowly, during which the solution turned bright red in color. The reaction mixture was extracted with CH_2Cl_2 (3 × 30 mL). The organic phase was dried over $MgSO_4$ and concentrated under reduced pressure. The resulting residue was purified using flash chromatography (n-Heptane/EtOAc 95/5) to afford 0.15 g (24 %) of the desired compound as a red oil (mixture of rotamers). $R_f = 0.43$ (n-Heptane/EtOAc 80/20); ^{1}H NMR (600 MHz, $CDCl_3$) δ 10.24 (s, 1H), 8.86 (s, 1H), 8.45 (s, 1H), 7.86 (s, 1H), 4.59–4.37 (m, 2H), 3.34–3.06 (m, 2H), 1.68–1.35 (m, 11H), 0.87 (t, $J = 7.3$ Hz, 3H); ^{13}C NMR (151 MHz, $CDCl_3$) δ 165.21, 158.02, 156.14, 155.32, 142.62, 142.37, 140.81, 140.59, 135.74, 133.47, 126.20, 95.11, 80.15, 49.97, 49.39, 48.94, 28.41, 21.53, 21.34, 11.26.

2.4.5. Tert-butyl (3-(1,2,4,5-tetrazin-3-yl)-5-(trimethylstannyl)benzyl)(ethyl)carbamate (14)

$Pd(PPh_3)_4$ (19.4 mg, 10 %) and hexamethylditin (87 μL, 0.42 mmol) were successively added to a microwave vial equipped with a stir bar which was then sealed and purged with N_2. 3-iodo-5-(1,2,4,5-tetrazin-3-yl)benzyl(propyl)carbamate (0.05 g, 0.11 mmol) in dry THF (2.5 mL) was added via a syringe and the reaction allowed to stir at 65 °C in a microwave for 2 h. The reaction was allowed to cool to room temperature and unsealed before being quenched with saturated aqueous KF (1 mL). The solution was extracted with CH_2Cl_2 washed with brine (2 × 5 mL), dried over $MgSO_4$, filtered and concentrated under reduced pressure. The tetrazine was then purified using flash chromatography (n-Heptane/EtOAc 90/10) to yield 0.025 g (46 %) of a purple oil (mixture of rotamers). $R_f = 0.48$ (n-Heptane/EtOAc 80/20); ^{1}H NMR (600 MHz, $CDCl_3$) δ 10.21 (s, 1H), 8.64 (d, $J = 22.2$ Hz, 1H), 8.48–8.27 (m, 1H), 7.72–7.58 (m, 1H), 4.64–4.45 (m, 2H), 3.35–3.05 (m, 2H), 1.63–1.39 (m, 11H), 0.88 (t, $J = 6.8$ Hz, 3H, partially covered by n-Heptane signal), 0.36 (s, 9H); ^{13}C NMR (151 MHz, $CDCl_3$) δ 166.76, 157.78, 156.27, 155.56, 144.46, 139.63, 139.34, 135.23, 134.24, 131.02, 127.04, 50.60, 49.97, 48.74, 28.45, 21.60, 21.26, 11.30, −9.37.

2.5. Synthesis of 3

2.5.1. Synthesis of 3-(bromomethyl)-5-fluorobenzonitrile (7)

To a solution of 3-fluoro-5-methylbenzonitrile (2.61 g, 19.24 mmol) and N-bromosuccinimide (5.13 g, 28.86 mmol) in CH_3CN was added AIBN (1.26 g, 7.69 mmol). The reaction was refluxed for 24 h. The solvent was removed under vacuum and the crude purified by flash chromatography (n-Heptane/EtOAc 95/5) to give 2.10 g (51 %) of 3-(bromomethyl)-5-fluorobenzonitrile as a colorless oil. $R_f = 0.32$ (n-Heptane/EtOAc 95/5); ^{1}H NMR (400 MHz, $CDCl_3$) δ 7.50 (t, $J = 1.5$ Hz, 1H), 7.38 (dt, $J = 8.9$, 2.0 Hz, 1H), 7.30 (ddd, $J = 7.9$, 2.5, 1.3 Hz, 1H), 4.46 (s, 2H); ^{13}C NMR (101 MHz, $CDCl_3$) δ 162.12 (d, $J = 251.3$ Hz),

141.93 (d, $J = 8.0$ Hz), 128.52 (d, $J = 3.4$ Hz), 121.06 (d, $J = 22.0$ Hz), 118.97 (d, $J = 24.7$ Hz), 117.07 (d, $J = 3.3$ Hz), 114.26 (d, $J = 9.9$ Hz), 30.32 (d, $J = 1.9$ Hz).

2.5.2. Synthesis of 3-((Propylamino)methyl)-5-fluorobenzonitrile hydrochloride (9)

To a solution of the 3-(bromomethyl)-5-fluorobenzonitrile (1.0 g, 4.67 mmol) in THF (25 mL) and was added propylamine (3.8 mL, 46.72 mmol). The reaction was stirred at room temperature for 5 h. The solution was concentrated and taken up with water (20 mL) and the resulting solution was extracted with CH_2Cl_2 (2 × 20 mL), washed with brine, dried with $MgSO_4$ and filtered before concentrating under reduced pressure to afford the free amine as a yellow oil. The compound was resolubilized in Et_2O and HCl in Et_2O was added. The solid obtained was filtered and crystallized from MeOH/Et_2O to give 0.92 g (86 %) of 3-fluoro-5-((propylamino)methyl)benzonitrile hydrochloride as a white solid. ^{1}H NMR (400 MHz, DMSO-d_6) δ 9.68 (s, 2H), 8.69–7.21 (m, 3H), 4.20 (s, 2H), 2.83 (t, $J = 7.8$ Hz, 2H), 1.70 (h, $J = 7.5$ Hz, 2H), 0.91 (t, $J = 7.4$ Hz, 3H); ^{13}C NMR (101 MHz, DMSO-d_6) δ 161.76 (d, $J = 247.2$ Hz), 137.04 (d, $J = 8.6$ Hz), 130.97 (d, $J = 3.3$ Hz), 123.15 (d, $J = 22.5$ Hz), 120.06 (d, $J = 25.3$ Hz), 117.80 (d, $J = 3.3$ Hz), 113.30 (d, $J = 10.5$ Hz), 48.80, 48.60, 19.35, 11.45.

2.5.3. Synthesis of tert-butyl (3-cyano-5-fluorobenzyl)(propyl)carbamate (11)

3-Fluoro-5-((propylamino)methyl)benzonitrile hydrochloride (0.85 g, 3.72 mmol) and triethylamine (1.55 mL, 11.16 mmol) were dissolved in anhydrous CH_2Cl_2 (30 mL) at 0 °C. To this stirred solution was added di-tert-butyl dicarbonate (0.89 g, 4.09 mmol), and the reaction allowed to warm to room temperature and stirred for 12 h. The reaction mixture was evaporated under reduced pressure, and the residue was re-dissolved in diethyl ether (40 mL), which was washed successively with 0.5 M aq. HCl (2 × 15 mL), saturated $NaHCO_3$ (2 × 15 mL) and brine (15 mL). The organic layer was dried over anhydrous $MgSO_4$, filtered and evaporated under reduced pressure to give a white solid. The residue was purified by flash chromatography (n-Heptane/EtOAc 85/15) to afford 1.05 g (97 %) of the desired compound as a colorless oil (mixture of rotamers). $R_f = 0.42$ (n-Heptane/EtOAc 80/20); ^{1}H NMR (400 MHz, $CDCl_3$) δ 7.31 (s, 1H), 7.26–7.09 (m, 2H), 4.43 (s, 2H), 3.14 (s, 2H), 1.48 (br s, 11H), 0.87 (t, $J = 7.4$ Hz, 3H); ^{13}C NMR (101 MHz, $CDCl_3$) δ 162.41 (d, $J = 250.6$ Hz), 155.97, 143.78, 131.88–124.65 (m), 119.14, 117.73 (d, $J = 25.0$ Hz), 113.85 (d, $J = 9.6$ Hz), 80.33, 49.45, 49.11, 28.35, 21.53, 11.20.

2.5.4. Synthesis of tert-butyl (3-fluoro-5-(1,2,4,5-tetrazin-3-yl)benzyl)(propyl)carbamate (13)

The compound was synthesized as previously reported [36]. T*ert*-butyl (3-cyano-5-fluorobenzyl)(propyl)carbamate (1.05 g, 3.59 mmol), CH_2Cl_2 (0.23 mL, 3.59 mmol), sulfur (0.23 g, 0.9 mmol), and ethanol (4.0 mL) were mixed together in a microwave reaction vial. Hydrazine monohydrate (1.4 mL, 28.73 mmol) was added dropwise with stirring. The vessel was sealed, and the reaction mixture was heated to 50 °C for 24 h. The reaction was diluted with 3 mL of CH_2Cl_2, and sodium nitrite (2.48 g, 35.91 mmol) in 30 mL of H_2O was added dropwise to the mixture under cooling. Excess acetic acid (14 mL) was then added slowly, during which the solution turned bright red in color. The reaction mixture was extracted with CH_2Cl_2 (3 × 30 mL). The organic phase was dried over $MgSO_4$ and concentrated under reduced pressure. The resulting residue was purified using flash chromatography (n-Heptane/EtOAc 95/5) to afford 0.36 g (29 %) of the desired compound as a red oil (mixture of rotamers). $R_f = 0.42$ (n-Heptane/EtOAc 80/20); ^{1}H NMR (400 MHz, $CDCl_3$) δ 10.23 (s, 1H), 8.29 (s, 1H), 8.19 (d, $J = 9.3$ Hz, 1H), 7.23 (d, $J = 8.9$ Hz, 1H), 4.53 (s, 2H), 3.18 (s, 2H), 2.03–1.20 (m, 11H), 0.86 (td, $J = 7.5$, 4.0 Hz, 3H); ^{13}C NMR (101 MHz, $CDCl_3$) δ 165.60 (d, $J = 3.4$ Hz), 163.52 (d, $J = 248.2$ Hz), 158.00, 156.12, 143.19, 133.68 (d, $J = 8.5$ Hz), 122.64, 118.83, 113.83 (d, $J = 24.2$ Hz), 80.06, 49.74, 48.94, 28.38, 21.48, 11.23.

2.5.5. N-(3-Fluoro-5-(1,2,4,5-tetrazin-3-yl)benzyl)propylamine hydrochloride (3)

To a solution of (3-fluoro-5-(1,2,4,5-tetrazin-3-yl)benzyl)(propyl) carbamate (0.30 g, 0.86 mmol) in CH_2Cl_2 (10 mL) was added a solution of HCl in dioxane (4.0 M, 5.0 mL). The mixture was stirred at room temperature for 2 h. The reaction was then concentrated under reduced pressure to give 0.22 g (90 %) of a pink solid. ^{1}H NMR (400 MHz, DMSO-d_6) δ 10.70 (s, 1H), 9.53 (s, 2H), 8.59 (s, 1H), 8.49–8.15 (m, 1H), 7.93 (dt, $J = 9.4$, 2.0 Hz, 1H), 4.34 (t, $J = 5.8$ Hz, H), 2.90 (dd, $J = 9.7$, 5.1 Hz, H), 1.71 (q, $J = 7.7$ Hz, 2H), 0.93 (t, $J = 7.5$ Hz, 3H); ^{13}C NMR (101 MHz, DMSO-d_6) δ 164.89, 162.76 (d, $J = 245.7$ Hz), 158.94, 136.74 (d, $J = 8.1$ Hz), 134.95 (d, $J = 8.6$ Hz), 126.12 (d, $J = 2.9$ Hz), 121.85 (d, $J = 22.5$ Hz), 115.14 (d, $J = 24.1$ Hz), 49.44, 48.70, 19.39, 11.48.

2.6. Radiochemistry

General information. Radiochemistry was performed at Department of Clinical Physiology, Nuclear Medicine & PET, Rigshospitalet, Denmark. [^{18}F]Fluoride was produced via the (p,n)-reaction in a cyclotron (60 μA CTI Siemens or 40 μA Scanditronix) by irradiating [^{18}O]H_2O with a 11 MeV (CTI siemens) or 16 MeV (Scanditronix) proton beam. Automated syntheses were performed on a Scansys Laboratorieteknik synthesis module housed in a hot cell. Analytical HPLC was performed on a Dionex system connected to a P680A pump, a UVD 170 U detector and a Scansys radiodetector. Semi-preparative HPLC was performed on the built-in HPLC system in the synthesis module and the flow rate was set to 4 mL/min at all times.

Identity of radiolabeled products was confirmed by comparing their radioactivity and UV absorbance traces on radio-HPLC with the UV traces of the corresponding ^{19}F-reference solutions. The radiochemical yield (RCY) was determined using the activity of [^{18}F]fluoride received from the cyclotron at the beginning of the synthesis and that of the HPLC purified product at the end of the synthesis, corrected for decay (d.c.). The molar activity (A_m) was determined from radioactivity concentration and total compound concentration in the formulated solution of the radiolabeled product. The former was determined with a dose calibrator, while the latter was estimated by comparing the integrated UV peak area of the product with peak areas obtained from standard solutions of the corresponding ^{19}F-reference on the HPLC chromatogram. The values for radiochemical yield (RCY), radiochemical purity (RCP) and molar activity (A_m) are given as mean values. This applies for all radiolabeled compounds described below.

2.6.1. Radiolabeling of [^{18}F]1

Synthesis of 1-azido-2-[^{18}F]fluoroethane: Irradiated [^{18}O]water containing [^{18}F]fluoride was passed through an anion exchange resin cartridge (Sep-Pak Accell Plus QMA Plus Light, chloride form). [^{18}F] Fluoride trapped on the QMA was then eluted with an aliquot (0.6 mL) of eluting solution (19 mg/mL 4,7,13,16,21,24-hexaoxa-1,10-diazabicyclo[8.8.8]hexacosane and 5 mg/mL K_2CO_3 in 96 % methanol) into a 4 mL glass vial. The resulting mixture was then gently evaporated to dryness at 100 °C under nitrogen flow. When the solvents evaporated, dry acetonitrile (0.5 mL) was added to the vial and also evaporated. Addition of acetonitrile with subsequent evaporation was repeated twice.

2-Azidoethyl 4-nitrobenzenesulfonate (3 mg, 11 μmol) dissolved in acetonitrile (0.5 mL) was added to dried [^{18}F]fluoride, and the mixture was heated for 2 min at 100 °C. After that, the reaction vial was connected with a 1/16" OD polypropylene line to a 7 mL condensation vial closed with a septum with a vent needle and containing sodium diphenylphosphinobenzene-3-sulfonate (4–5 mg, 11–14 μmol) dissolved in aqueous sodium hydroxide solution (20 mM, 0.5 mL). A long 21G needle was inserted into the reaction vial, reaching to the bottom, and a

flow of nitrogen was applied through the needle to facilitate the distillation of 1-azido-2-[^{18}F]fluoroethane and acetonitrile from the reaction vial and condensation in the condensation vial. The distillation was performed for 5 min, during which the reaction vial was heated to 80 °C, while the condensation vial was cooled to 20 °C. In situ reduction of 1-azido-2-[^{18}F]fluoroethane to 1-amino-2-[^{18}F]fluoroethane: at the end of 1-azido-2-[^{18}F]fluoroethane distillation, the polypropylene line and the vent needle were removed from the condensation vial, and the vial was heated at 100 °C for 15 min. Coupling to tetrazine NHS ester: 2,5-dioxopyrrolidin-1-yl 2-(4-(1,2,4,5-tetrazin-3-yl)phenyl)acetate (2.4 mg, 8 μmol) was dissolved in DMF (0.1 mL), diluted with acidified phosphate buffer (0.1 mL of 0.1 M buffer solution pH 7 mixed with 5 μL 1 M HCl), added to the 1-amino-2-[^{18}F]fluoroethane solution in the condensation vial and left to react for 4 min at room temperature. The reaction mixture was diluted with water (1.5 mL) and purified by HPLC using Luna 5 μ C18(2) 100 Å 250 × 10 mm column eluted with the 40/60 *v*/v mixture of acetonitrile and potassium dihydrophosphate buffer (50 mM, pH 6.1). The flow rate was 4 mL/min. The HPLC fraction containing [^{18}F]**1** (retention time 7.2 min) was diluted with water (50 mL) and loaded on a Sep-Pak C18 Plus Light cartridge. The cartridge was flushed with extra water (2 mL) and eluted with 96 % ethanol (1 mL). The eluate was diluted with 20 mL phosphate buffer (100 mM, pH 7).

2.6.2. Radiolabeling of [^{18}F]*3*

Radiosynthesis of [^{18}F]**3** is described in [34]. Briefly, a stannane precursor was labeled with ^{18}F via a copper-mediated ^{18}F-fluorodestannylation, and then Boc protection was removed from the secondary amino group by heating in TFA/acetonitrile mixture (ca. 30 % vol. TFA).

2.6.3. $LogD_{7.4}$ determinations

Following the synthesis and HPLC purification of [^{18}F]**1** or [^{18}F]**3**, the HPLC fraction containing the respective tetrazine was diluted with water and loaded onto a Sep-Pak C18 Plus Light cartridge (Waters, USA) pre-activated with 50 % ethanol (5–7 mL). The Sep-Pak cartridge was dried in strong nitrogen flow for approx. 1 min and eluted with 1 mL of n-octanol. Aliquots of the eluate (2 × 10 μL) were added to two Eppendorf tubes containing 500 μL of phosphate buffer (100 mM, pH 7.2) and 490 μL n-octanol each. The solutions were then vortexed for 5 min, followed by centrifugation (3000 xg) for 10 min. Subsequently, 3 × 100 μL aliquots were taken from both the organic and water phases of both Eppendorf tubes. The radioactivity contained in the aliquots was measured in a gamma counter (Packard Cobra, US) using energy window of 461–561 keV. The LogD value was then calculated by taking the decimal logarithm of the ratios between the activities measured for the organic and the water phases.

2.7. Pretargeted autoradiography

Full autoradiography protocol is described in [34]. In short, sagittal brain slices from tg-ArcSwe mice that express human Aβ were mounted on Superfrost adhesive slides and incubated overnight with TCO-modified 3D6 anti-Aβ antibody (ca. 7 TCO per antibody). Two antibody concentrations were used: 0.006 μg/mL and 0.06 μg/mL. Afterwards, the unbound antibody was washed away, and the slices were incubated with 20 nM [^{18}F]Tz for 1 h, rinsed with demineralized water, dried and exposed on phosphor storage screens. The phosphor storage screens were read on a Cyclone Storage Phosphor System (Packard Instruments Co). Quantification of plate readings was done with Optiquant software (version 3.00, Packard Instruments Co) and ImageJ by drawing regions of interest on the cortex and cerebellum manually.

2.8. In vivo evaluation

2.8.1. Animals

Long-Evans female rats weighing 200–300 g (Charles River, Calco, Italy), were housed in a cage of 2–3 rats per cage and kept in a climate-controlled facility with a 12-h light/dark cycle. The cages had environmental enrichment (nest box, biting stick). All rats were fed ad libitum with commercial breeding diet (1310 FORTI- Avlsfoder, Brogaarden, Altromin International) and had free access to water. All animal experiments were performed in accordance with the European Commission's Directive 2010/63/EU for animal research and with approval from The Danish Council for Animal Ethics (license numbers 2017-15-0201-01283 and 2017-15-0201-01375) together with the Department of Experimental Medicine, University of Copenhagen.

2.8.2. Experimental set-ups

Three experimental set-ups were used for in vivo evaluation of [^{18}F]Tzs. For assessment of brain uptake and washout kinetics, groups of intact rats (n = 2 per tetrazine) received intravenous injections of [^{18}F]Tzs and were subjected to a 90-min-long dynamic PET scan from the moment of injection. For assessment of in vivo click performance of the [^{18}F]Tzs, rats (n = 3 per tetrazine) were injected intracerebrally with TCO-Peptobrush polymer and allowed to recover for 24 h. Afterwards, the rats also received intravenous injections of [^{18}F]Tz and were scanned in the PET scanner for 90 min. Finally, for the evaluation of in vivo metabolism of [^{18}F]Tzs, intact rats (n = 3 per tetrazine) with arterial cannulas were injected intravenously with [^{18}F]Tzs, arterial blood samples were drawn over the period of 1 to 90 min post-injection and analyzed for radiometabolites content.

2.8.3. PET procedure

PET imaging was performed on the Siemens HRRT (High-Resolution Research Tomography) (CPS Innovations/Siemens, Malvern, PA, USA). On the day of experiment, the rats were weighed and then transported to the scanner at least 2 h before the scan. Anesthesia was induced using 3 % isoflurane in oxygen flow. All rats were placed in a 2 × 2 custom made rat holder, enabling simultaneous scanning of four rats. While in the custom-made rat holder, the rats were kept under anesthesia with a constant flow of isoflurane (~2 % isoflurane in oxygen). The rats were cannulated in the dorsal or lateral tail vein with BD Neoflon 24G vein catheter and flushed with a solution of 4 unit/mL heparin in saline. The rats were placed in the scanner and kept warm using an infrared lamp or heating pads and checked for respiration throughout the entire scan. [^{18}F]**1** or [^{18}F]**3** (5–25 MBq, 0.12–0.3 nmol in 0.5–1.0 mL) was injected through the catheter and a 90 min PET acquisition (emission scan) was started at the time of injection. A rotating point source ^{137}Cs transmission scan was carried out before or after each emission scan.

2.8.4. Intracerebral TCO-polymer injection

The full procedure for intracerebral TCO-polymer injection was recently reported [34]. In short, 4 μL of TCO-PeptoBrush polymer solution (25 mg/mL in PBS) were injected into the right striatum through a hole drilled in the skull. Total injected polymer amount was 100 μg, corresponding to 15 nmol TCO.

TCO-polymer was labeled with indium-111 (^{111}In) to allow quantification of polymer retained at injection site by ex vivo gamma counting. TCO-polymer labeling is described in detail in [34], Briefly, 1,4,7,10-tetraazacyclododecane-1,4,7,10-tetraacetic acid (DOTA)-PEG_{11}-tetrazine was incubated with [^{111}In]$InCl_3$ in ammonium acetate buffer (0.2 M pH 5.5) at 60 °C for 5 min, which led to >95 % chelation of ^{111}In. The resulting [^{111}In]In-DOTA-tetrazine solution (50–60 nmol/mL, 500–600 MBq/mL) was then diluted 2000-fold with 10 mM phosphate-buffered saline and mixed with an equal volume of TCO-polymer solution (7.5 mmol TCO per mL) in phosphate-buffered saline. [^{111}In]In-DOTA-tetrazine quantitatively clicked to the huge excess of TCO groups, and the resulting mixture was used for intracerebral injections.

Pretargeted PET imaging was performed 24 h after TCO-polymer injection. After the scan, the rats were sacrificed by decapitation, brains were extracted and cut into two halves along the sagittal symmetry plane. Left and right brain halves were put into gamma counting

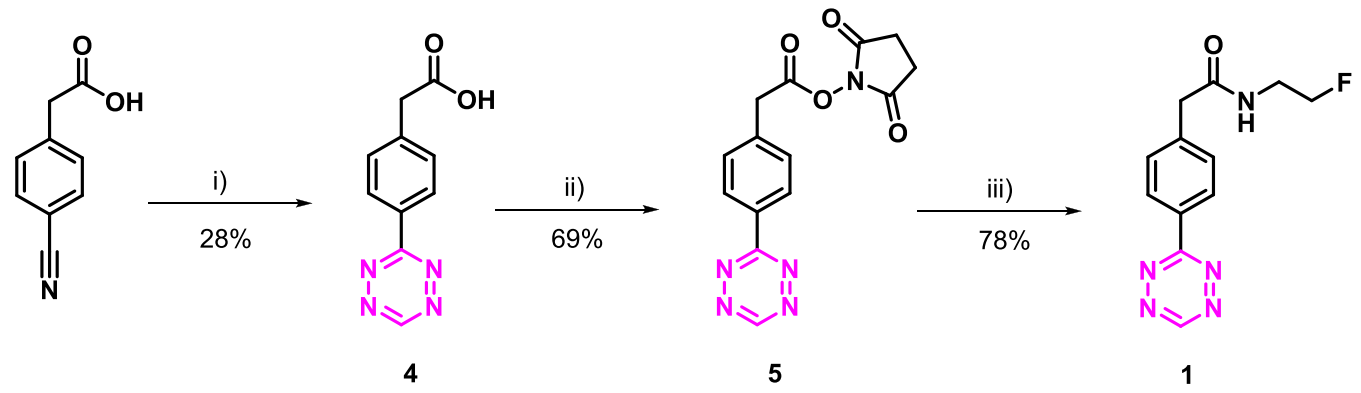

Scheme 1. Synthesis of Tz **1** and its precursor **5**. *Reagents and conditions:* i) a) CH_2Cl_2, S_8, $NH_2NH_2 \cdot H_2O$, EtOH, 50 °C, 24 h; b) $NaNO_2$, AcOH, 0 °C, 10 min; ii) NHS, DCC, THF, rt., 12 h; iii) $F(CH_2)_2NH_2 \cdot HCl$, Et_3N, THF, rt., 6 h.

tubes, left at 4 °C for 24 h to ensure full decay of ^{18}F and then counted on the gamma counter to measure the amount of ^{111}In activity in the brain halves. Aliquots of ^{111}In-labeled PeptoBrush solution used for intracranial injections (4 μL, same as injected volume) were counted along with brain halves to calculate the fraction of injected ^{111}In activity retained in the brain halves.

2.8.5. Data analysis

PET list-mode emission files were reconstructed with the aid of ordinary Poisson 3D subset expectation maximization (OP-3D-OSEM) algorithm, including modeling the point-spread function, with 16 subsets, ten iterations, and standard corrections. The transmission attenuation map was regenerated using maximum posteriori algorithm. Emission data were binned into time frames of increasing lengths: 6 × 10 s, 8 × 30 s, 5 × 60 s and 16 × 300 s. Each reconstructed time frame image consisted of 207 planes of 256 × 256 voxels of 1.22 × 1.22 × 1.22 mm size.

To analyze the data, the program PMOD 3.7 (PMOD Technologies, Zürich, Switzerland) was used. A standard rat brain MRI atlas was used to extract the preferred volumes of interest (VOIs). The time-activity curves (TACs) from all the collected VOIs were converted into percentage injected radioactivity dose per mL tissue (ID%/mL).

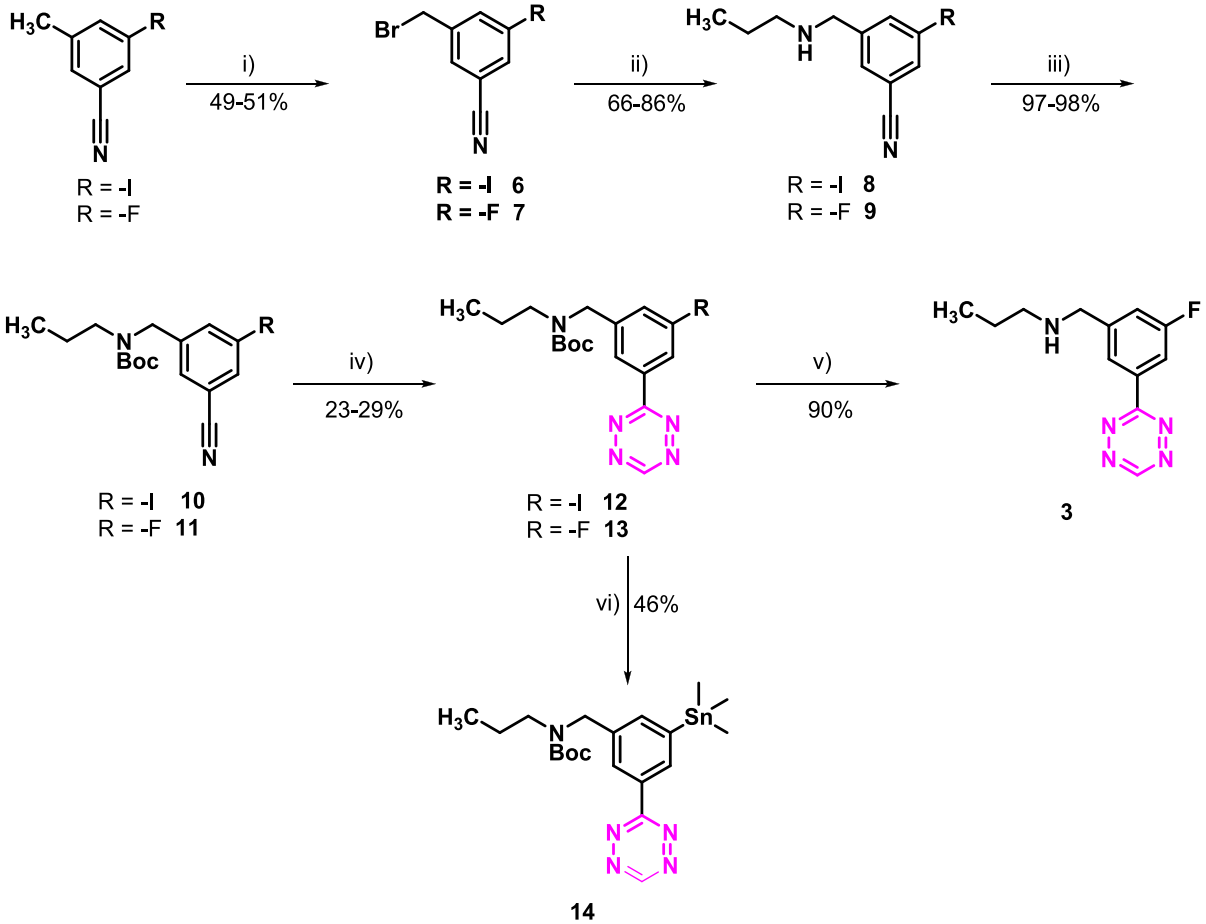

Scheme 2. Synthesis of Tz **3** and its precursor **14.** *Reagents and conditions: i*) NBS, AIBN, CH_3CN, reflux 12 h; *ii*) NH_4OH, THF, 50 °C, 5 h; iii) Boc_2O, Et_3N, CH_2Cl_2, rt., 12 h; iv) a) CH_2Cl_2, S_8, $NH_2NH_2 \cdot H_2O$, EtOH, 50 °C, 24 h; b) $NaNO_2$, AcOH, 0 °C, 10 min; v) HCl, dioxane, rt., 2 h; vi) $(Me_3Sn)_2$, $Pd(PPh_3)_4$, THF, 65 °C, MW, 2 h.

Table 1
Overview of the physicochemical properties and reactivity of **1** and **3**.

Tetrazine	1	3
MW (g/mol)[a]	261	247
$clogD_{7.4}$[b]	−0.14	−0.79
Experimental $logD_{7.4}$	0.81	0.27
TPSA[c]	80.7	63.6
H-bond acceptor	5	5
H-bond donor	1	1
CNS MPO score[d]	5.83	5.99
BBB score[e]	4.26	4.43
Rate constants (M^{-1} s^{-1}) (in DPBS @ 37 °C)[f]	57,000	73,000

[a] Molecular weight.
[b] $clogD_{7.4}$ = distribution coefficient at physiological pH (7.4) calculated with Chemicalize.
[c] Topological polar surface area.
[d] Central nervous system multiparameter optimization score [37].
[e] Blood-brain-barrier score [38].
[f] Second order rate constants are estimated from measurements of the Tz structural classes with trans-cyclooctene (TCO) in Dulbecco's Phosphate Buffered Saline [26,34].

2.8.6. *In vivo metabolism in healthy rats*

Healthy female Sprague-Dawley rats were anesthetized with a mixture of isoflurane/air (inhalation anesthesia, 5 % ratio during induction, 2 % at maintenance). The body temperature of the anesthetized animals was maintained by placing them on warming pads. One of the femoral arteries and one lateral tail vein of each rat were cannulated. Arterial cannulations were carried out with 0.61 mm OD PE10/10 tubing ([^{18}F]**1**) or 0.9 mm OD PE50 tubing ([^{18}F]**3**). Venous cannulations were carried out with BD Neoflon 24G vein catheters. Catheters and cannulas were flushed with a solution of 100 unit/mL heparin in saline. The cannulations took 40–50 min.

After the cannulation, [^{18}F]Tz ([^{18}F]**1** or [^{18}F]**3)** in 0.1 M pH 7 phosphate buffer (10–20 MBq, 0.25–0.5 nmol in 0.4–0.5 mL) was injected through the venous catheter, and arterial blood samples of 0.10–0.15 mL were withdrawn through the arterial cannula right before [^{18}F]Tz injection (spiking sample) and at 1, 2, 5, 10, 15, 20, 40, 60 and 90 min after [^{18}F]Tz injection.

From collected whole blood samples, 25 μL aliquots were withdrawn for gamma counting, while the rest of the blood was centrifuged at 4000 *g* for 5 min, and two 25 μL aliquots were withdrawn from the obtained supernatant (plasma) samples. One set of plasma aliquots was used for gamma counting, while another set was used for radiometabolite analysis. Gamma counting was performed on Hidex gamma counter for [^{18}F]**1** and Packard Cobra counter for [^{18}F]**3**. Aliquots of injected [^{18}F]Tz solution were counted along with the blood/plasma samples to convert counts into %ID/mL.

For radiometabolite analysis, plasma aliquots (25 μL) were mixed with 75 μL of acetonitrile to precipitate proteins. From the resulting 100 μL, 6 μL portions were withdrawn for radio-TLC to analyze radiometabolite content. Radio-TLC analysis was performed on silica plates. Plasma obtained from the spiking samples (before [^{18}F]Tz injection) was

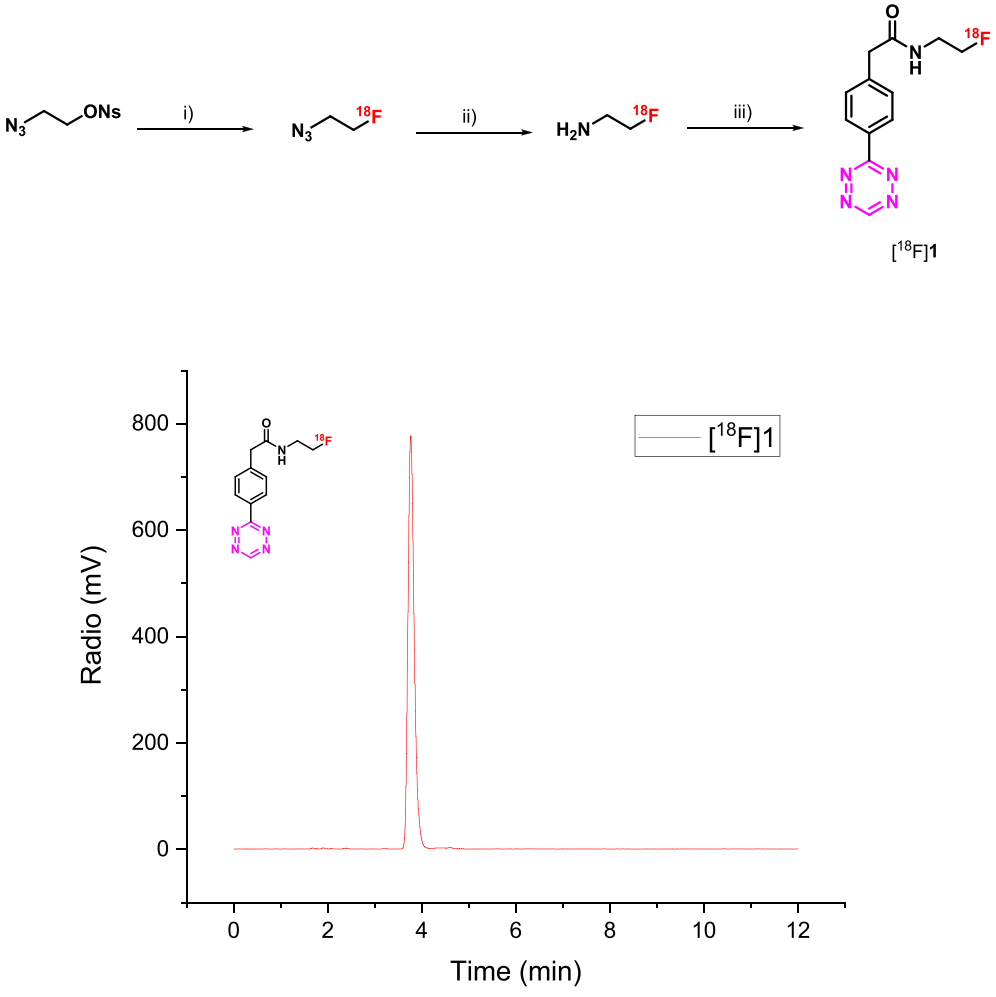

Scheme 3. Upper: Radiolabeling of [^{18}F]**1.** *Reagents and conditions: i)* [^{18}F]KF, Kryptofix, CH_3CN, distillation at 80–100 °C, 7 min; ii) sodium diphenylphosphinobenzene-3-sulfonate, aq. NaOH, 100 °C, 15 min; iii) **5**, DMF/water buffered to pH ≈ 7, r.t., 4 min. Lower: HPLC chromatogram of purified [^{18}F]**1**.

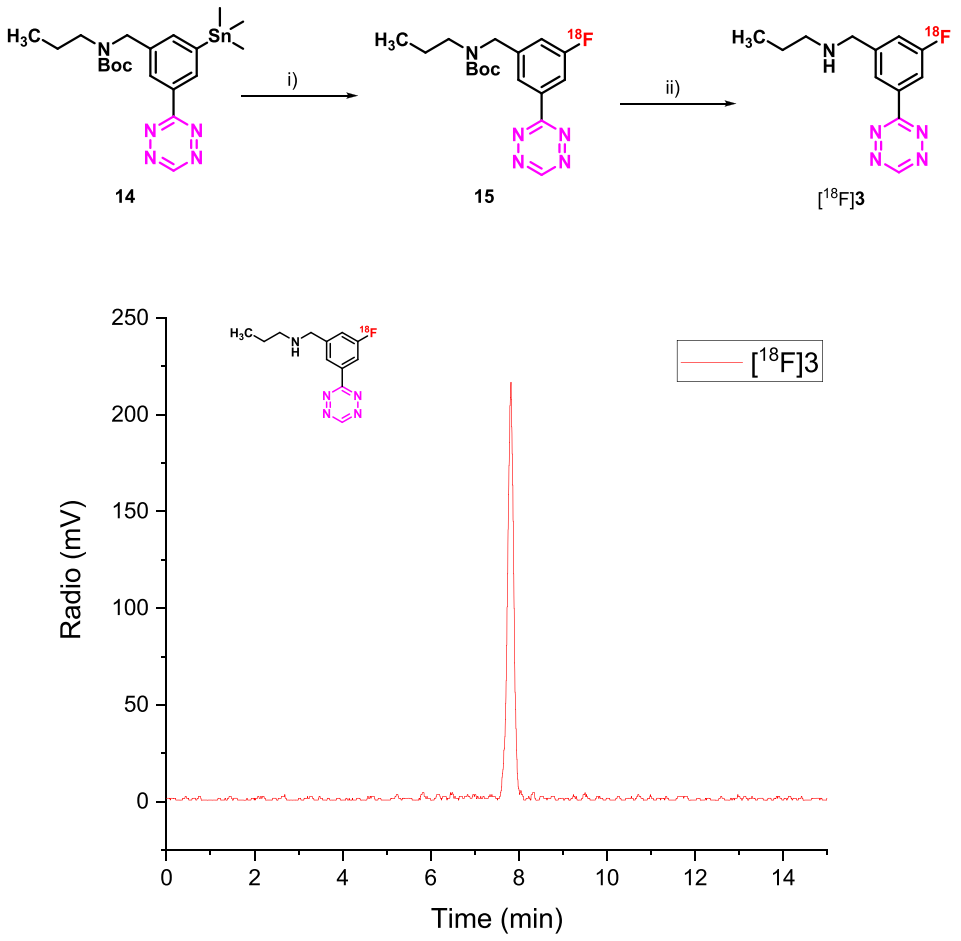

Scheme 4. Upper: Radiolabeling of [^{18}F]**3**. *Reagents and conditions: i)* [^{18}F]KF, Cu(OTf)$_2$, pyridine, DMA, 100 °C, 5 min; ii) CH_3CN/TFA, 80 °C, 10 min. Lower: HPLC chromatogram of formulated [^{18}F]**3**.

spiked with [^{18}F]Tz solution used for injection and worked up in the same manner. Spiking samples were run on radio-TLC plates along with the other samples to confirm the identity of the parent compound in plasma. TLC conditions and examples of chromatograms are shown in Table S1 and Fig. S3, respectively.

3. Results and discussion

3.1. Synthesis of precursors and references

Both compounds and their respective precursors were synthesized similarly to previously reported procedures (Schemes 1 and 2) [29,34]. The synthesis of compound **1** and its precursor **5** is quite straightforward. Briefly, Tz **4** can be obtained using a metal-free synthetic approach reported by Qu et al. (Scheme 1) [36]. The latter is converted to the corresponding NHS-ester **5** under standard conditions. Finally, coupling with 2-fluoroethylamine hydrochloride gave the desired compound **1**.

The synthesis of compound **3** and its precursor **14** is lengthy and more complex due to the lack of commercially available intermediates. In particular, Boc-protected nitriles for the synthesis of Tzs **12** and **13** were obtained by reacting the corresponding bromobenzyl compounds (**6** and **7**) with propylamine. The primary amines were then reacted with di-*tert*-butyl dicarbonate to afford the protected compounds **10** and **11** (Scheme 2). These were converted to the tetrazine analogues using the conditions above mentioned for **1**. Finally, compound **12** was converted to the trimethylstannane analogue by Pd catalyzed Stille coupling while **13** was deprotected under acidic conditions to yield **3**.

3.2. Comparison of physicochemical properties and reactivity

The structure of probes **1** and **3** is similar, i.e., it consists of a reactive aryltetrazine core. Both compounds have similar polarity, MW and TPSA (Table 1). They both show very promising CNS MPO and BBB scores confirming their ability to enter the brain in sufficient amounts [37,38]. The Tzs have adequate reaction kinetics for in vivo applications when undergoing an inverse electron-demand Diels–Alder reaction with TCO with compound **3** being more reactive due to the inductive effect of the fluorine atom and the substitution pattern [26,39]. Overall, Tz **3** shows a slightly better profile and as such, it may have better imaging properties.

3.3. Radiochemistry

Radiolabeling of [^{18}F]**1** was performed using the reported procedure with minor modifications (Scheme 3) [29]. In particular 2-azidoethyl 4-nitrobenzenesulfonate was reacted with ^{18}F to give 2-[^{18}F]fluoroethyl azide [40]. The latter was then reduced to [^{18}F]fluoroethylamine via Staudinger reaction and coupled with NHS ester **5** to give the final product [^{18}F]**1** [41]. The compound was obtained with a RCY of 3–16 % (here and further, range of values from 4 independent repetitions is given), RCP ≥98 % and an A_m of 24–97 GBq/μmol at end of synthesis. The isolated radioactivity amount of [^{18}F]**1** was 212–1170 MBq. The total synthesis time was approximately 100 min.

Tz [^{18}F]**3** was obtained via Cu-mediated ^{18}F-fluorination of a stannane precursor **14** in a one-pot, two-step synthesis using our previously reported method (Scheme 4) [31]. Radiosynthesis lasted 90 min and provided [^{18}F]**3** with a RCY of 12 ± 2, RCP ≥ 98 % and a A_m of 207 ± 7

A)

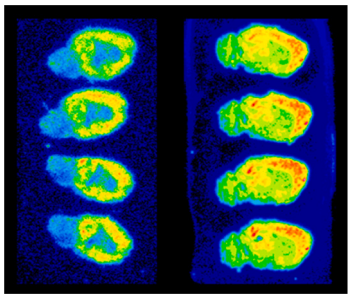

B)

Tetrazine	Cor/Cer ratio	
	0.06 μg/mL TCO-Ab	0.006 μg/mL TCO-Ab
[18F]**1**	1.30	2.59
[18F]**3**	1.09[a]	2.11[a]

Fig. 2. Evaluation of [18F]**1** and [18F]**3** by pretargeted autoradiography. A) Autoradiography images at high (0.06 μg/mL) TCO-Ab concentration. B) Cortex/cerebellum uptake ratios. [a] Previously published data [34].

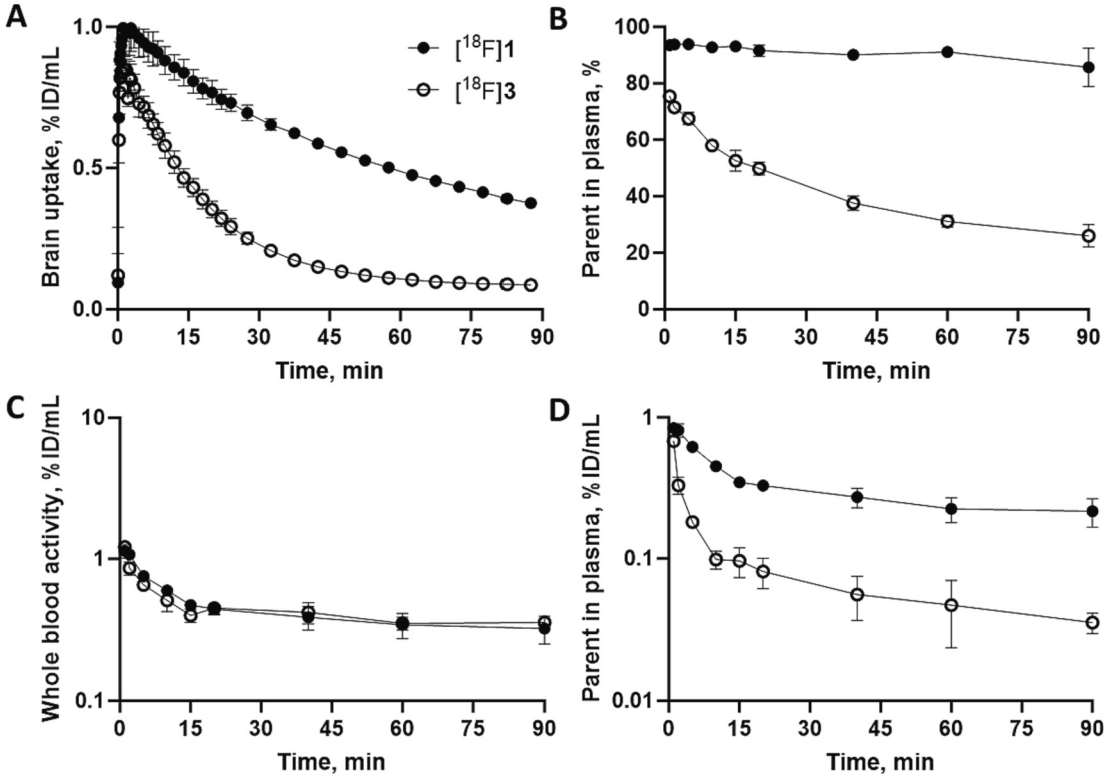

Fig. 3. In vivo evaluation of [18F]**1** and [18F]**3** in intact rats. A) Averaged time-activity curves for whole brain (n = 2 per Tz). B) Relative abundance (%) of unmetabolized parent in plasma. C) Average time-activity curves for total activity in whole arterial blood. D) Metabolite-corrected time-activity curves for arterial plasma. Curves in B-D represent averaged data from 3 rats per Tz. The data for compound [18F]**3** were previously published [34].

GBq/μmol.

After purification, both Tzs were formulated in ethanol/phosphate buffer (0.1 M, pH 7.4). Stability studies revealed that both compounds were stable for at least 2 h.

3.4. Pretargeted autoradiography

Autoradiography on tissue slices containing the target for imaging is a convenient method to identify radioligands with suitable imaging contrast for further in vivo studies. As Tzs do not possess a native target within the brain, direct autoradiography cannot be carried out. Therefore, we developed an autoradiography protocol based on pretargeting. We aimed to compare tetrazines in terms of their specific to non-specific binding ratios in brain tissue with standardized amount of TCO target introduced into it. For this setup, we used brain slices from tg-ArcSwe mice having a high concentration of Aβ fibrils in the cortex. TCO target, that would lead to irreversible specific binding of 18F-labeled tetrazines, was introduced into the tissue by incubating these slices with TCO-modified Abs against Aβ. The protocol is described in detail elsewhere [34]. Briefly, TCO-modified Abs were pre-adsorbed at two different concentrations (0.06 μg/mL and 0.006 μg/mL) on brain slices from tg-ArcSwe mice. The slices were then incubated with 20 nmol/L [18F]**1** or [18F]**3** to allow the Tzs to click to the Aβ-bound TCO-Abs. The uptake values in cortex (Cor, Aβ-rich region) and in cerebellum (Cer, Aβ-poor region, assumed to represent non-specific binding of Tzs) were determined. Cor/Cer uptake ratios for [18F]**1** and [18F]**3** were comparable to each other, with somewhat higher values for [18F]**1** at both TCO-Ab concentrations, apparently due to lower relative uptake in the cerebellum (Fig. 2).

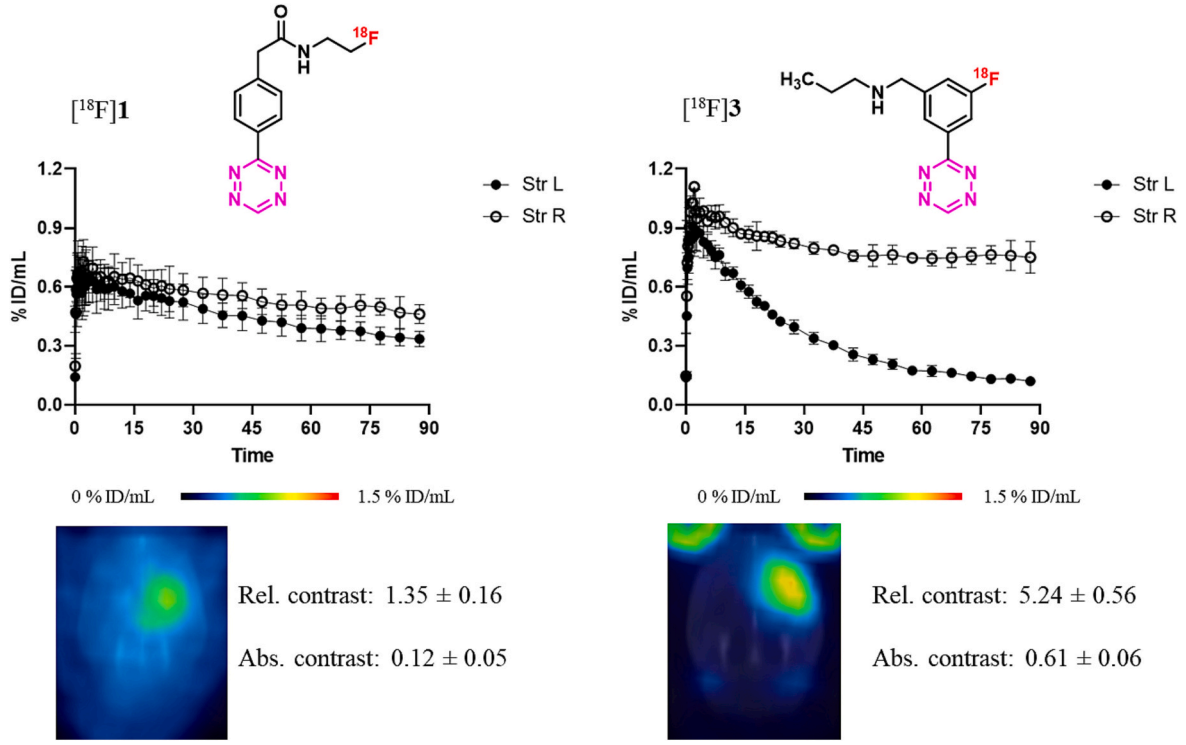

Fig. 4. In vivo click performance of [^{18}F]**1** and [^{18}F]**3** in the intracerebral TCO-polymer injection model. Upper: Average time-activity curves for left (polymer-free) and right (polymer-injected) striatum (n = 3). Lower: Horizontal sections of summed PET images for 60–90 min post-injection and relative/absolute contrast measurements. The data for compound [^{18}F]**3** were previously published data [34].

3.5. *In vivo evaluation*

In vivo evaluation of [^{18}F]**1** and [^{18}F]**3** consisted of two parts: assessment of brain uptake and washout kinetics in healthy intact Long-Evans rats and evaluation of the in vivo click performance of [^{18}F]**1** and [^{18}F]**3** to an intracerebral injected TCO-containing polymer in the same wild type animals.

Brain time-activity curves for the two Tzs are presented in Fig. 3A. [^{18}F]**1** and [^{18}F]**3** have comparable peak uptake values (1.03 ± 0.09 % ID/g and 0.86 ± 0.04 %ID/g, respectively), but the washout of [^{18}F]**3** appears to be much faster. After 90 min post-injection brain uptake differs 4-fold: 0.38 ± 0.01 %ID/g for [^{18}F]**1** and 0.09 ± 0.01 %ID/g for [^{18}F]**3**. Observed brain time-activity curve for [^{18}F]**1** is well in agreement with the values reported by Cook et al.: peak brain uptake and brain uptake at 60 min post-injection were, respectively, 2.51 ± 0.19 and 1.22 ± 0.01 in our hands and approximately 2.2 and 1.4 in Cook et al.'s data [29].

In our previous work, we used the ratio between peak brain uptake and area under the curve for brain uptake over 90 min post-injection, which we called uptake-washout index, as an outcome measure to rank tetrazines in terms how favorable their brain uptake and washout kinetics should be for pretargeted brain imaging [34]. The reasoning behind this index is that the best imaging contrast should be achieved if a Tz can reach a high concentration in the brain for an efficient click performance, and if the unreacted Tz can quickly be removed from the brain tissue when not reacted. The latter should result in a low background signal. The uptake-washout indices of [^{18}F]**1** and [^{18}F]**3** are 0.019 and 0.039, respectively, indicating that the uptake kinetics of [^{18}F]**3** is more favorable. Examination of radioactivity uptake in peripheral tissues showed that [^{18}F]**1** is cleared primarily through the kidneys, while [^{18}F]**3** is cleared through both kidneys and liver (Fig. S1). Concrete excretion pathways of radiotracers are less important for brain imaging than for the imaging of peripheral tissues, because the brain is located far away from either of the excreting organs. Therefore, in terms of peripheral tissue uptake neither of the Tzs had an advantage over the other.

Examination of in vivo metabolism data (Fig. 3B) shows that, within 90 min post-injection, the intended time period for imaging, most of plasma activity for [^{18}F]**1** corresponds to unmetabolized parent, while [^{18}F]**3** is extensively metabolized throughout the same time period, with only a bit over 20 % corresponding to unmetabolized parent by 90 min. Likewise, although time-activity curves for whole arterial blood are almost identical for the two Tzs (Fig. 3C), metabolite-corrected time-activity curve for arterial plasma lies much lower for [^{18}F]**3** than for [^{18}F]**1**. The main radiometabolite of [^{18}F]**3** is much more hydrophilic than [^{18}F]**3** itself (Fig. S3). Therefore, this radiometabolite is unlikely to penetrate the BBB, and the observed brain uptake for [^{18}F]**3** probably mostly represents intact [^{18}F]**3**. All in all, in vivo metabolism data suggest that faster washout of [^{18}F]**3** from the brain compared to [^{18}F]**1** can stem from the conversion of the former into a hydrophilic radiometabolite.

The results of the evaluation of [^{18}F]**1** and [^{18}F]**3** in the in vivo pretargeted imaging model with intrastriatally injected TCO-polymer are presented in Fig. 4, while polymer retention measurements are found in Supporting Information (Fig. S2). Preferential uptake of radioactivity in the polymer-injected striatum is visible on summed images for both compounds but is considerably more prominent for [^{18}F]**3**. Both relative and absolute imaging contrast, defined as, respectively, ratio and difference between radioactivity uptake in polymer-injected and polymer-free striata averaged over 60–90 min post-injection, were higher for [^{18}F]**3** than for [^{18}F]**1**.

In the original evaluation of [^{18}F]**1** by Cook et al., the average brain uptake of radioactivity was compared in naïve rats and in rats pretreated intrathecally with 560 μg of TCO-oligonucleotide (approximately 80 nmol TCO). At 60 min post-injection, the brain uptake in TCO-injected rats was 1.23-fold higher than in naïve rats [29]. It is hard to compare local TCO concentrations in our and Cook's pretargeted imaging setups, because we injected a lower molar amount of TCO-

Table 2
Summary of the properties and data of [^{18}F]**1** and [^{18}F]**3**.

	[^{18}F]1	[^{18}F]3
Chemical properties	*Suitable for CNS pretargeting*	*Suitable for CNS pretargeting*
Organic synthesis	*Simple, intermediates commercially available*	*Complex and time consuming*
Radiolabeling	*Complex, it requires a distillation step*	*One-pot two steps procedure*
In vitro stability	*Stable for shipment*	*Stable for shipment*
Autoradiography	*Higher contrast*	*Lower contrast*
Brain uptake	*~ 1 %ID/mL*	*~ 1 %ID/mL*
In vivo metabolism	*Almost no metabolism*	*Extensive metabolism*
Washout	*Slow*	*Fast*
In vivo imaging	*Lower contrast*	*Higher contrast*

polymer (15 nmol TCO) into the brain, but the injected polymer was distributed across a smaller volume. Nevertheless, calculating the right-to-left striatum uptake ratio at 60 min post-injection in our PET data for [^{18}F]**1** provides a value of 1.28. Therefore, our experimental setup and experimental setup used at Biogen appear to have similar signal-to-noise ratios in the evaluation of pretargeted imaging properties of radiolabeled tetrazines.

While showing promising results in rats, [^{18}F]**1** did not perform well in non-human primates due to insufficient clearance [29]. Given that [^{18}F]**3** showed considerably faster clearance from brain in rats, and consistently outperformed [^{18}F]**1** in our pretargeted imaging model, [^{18}F]**3** appears to be the best candidate for additional pretargeting studies.

4. Conclusion

We have evaluated the properties, synthesis, labeling and the in vitro/in vivo performance of [^{18}F]**1** and [^{18}F]**3** (Table 2). The physiochemical properties of both Tzs are suitable for CNS PET probes, and both have sufficient reactivity for pretargeted imaging. The precursor of [^{18}F]**1** and the relative "cold" reference can be easily obtained and some intermediated are commercially available. Differently, compound **3** and the relative precursor require several synthetic steps. However, the radiolabeling of [^{18}F]**1** is complex, time consuming and requires a distillation step, while [^{18}F]**3** can be labeled in higher yields, comparable purity and shorter time using a simpler protocol. Both Tzs have sufficient stability for shipment to short distances after formulation. The compounds showed comparable behavior in autoradiography experiments, but [^{18}F]**3** demonstrated considerably faster clearance from the brain in vivo, while having approximately the same peak uptake as [^{18}F]**1**, which can at least in part be attributed to the extensive conversion of [^{18}F]**3** into a hydrophilic radiometabolite. Therefore, pretargeted imaging with [^{18}F]**3** in rats provided higher contrast than [^{18}F]**1**, making [^{18}F]**3** a more promising candidate for further optimization and/or pretargeted imaging in larger animals.

CRediT authorship contribution statement

Vladimir Shalgunov: Writing – review & editing, Writing – original draft, Visualization, Validation, Supervision, Methodology, Investigation, Data curation, Conceptualization. **Sara Lopes van den Broek:** Visualization, Validation, Software, Methodology, Formal analysis, Data curation. **Ida Vang Andersen:** Visualization, Validation, Methodology, Formal analysis, Data curation. **Nakul R. Raval:** Methodology, Formal analysis, Data curation. **Gabriela Schäfer:** Resources, Methodology. **Matthias Barz:** Supervision, Resources, Funding acquisition. **Matthias M. Herth:** Writing – review & editing, Writing – original draft, Validation, Supervision, Project administration, Funding acquisition, Conceptualization. **Umberto M. Battisti:** Writing – review & editing, Writing – original draft, Visualization, Validation, Supervision, Project administration, Methodology, Investigation, Conceptualization.

Declaration of competing interest

The authors declare that they have no known competing financial interests or personal relationships that could have appeared to influence the work reported in this paper.

Acknowledgements

Stina Syvänen and Dag Sehlin (Uppsala University) are acknowledged for kindly providing the 3D6 antibody and the tg-ArcSwe brain tissue. This project has received funding from the European Union's EU Framework Programme for Research and Innovation Horizon 2020, under grant agreement no. 668532. MMH has received funding from the European Union's EU Framework Programme for Research and Innovation Horizon 2020 (grant agreement no. 670261). VS was supported by BRIDGE – Translational Excellence Programme at the Faculty of Health and Medical Sciences, University of Copenhagen, funded by the Novo Nordisk Foundation (grant agreement no. NNF18SA0034956). The Lundbeck Foundation, the Novo Nordisk Foundation, the Innovation Fund Denmark, and the Research Council for Independent Research (grant agreement no. 8022-00187B) are further acknowledged.

Appendix A. Supplementary data

Supplementary data to this article can be found online at https://doi.org/10.1016/j.nucmedbio.2024.108877.

References

[1] Stéen EJL, Edem PE, Nørregaard K, Jørgensen JT, Shalgunov V, Kjaer A, et al. Pretargeting in nuclear imaging and radionuclide therapy: improving efficacy of theranostics and nanomedicines. Biomaterials 2018;179:209–45.
[2] Altai M, Membreno R, Cook B, Tolmachev V, Zeglis BM. Pretargeted imaging and therapy. J Nucl Med 2017;58:1553–9.
[3] Bauer D, Cornejo MA, Hoang TT, Lewis JS, and Zeglis BM. Click chemistry and radiochemistry: an update. Bioconjugate Chemistry 2023, published on line.
[4] Devaraj NK. The future of bioorthogonal chemistry. ACS Central Science 2018;4:952–9.
[5] Oliveira BL, Guo Z, Bernardes GJL. Inverse electron demand Diels–Alder reactions in chemical biology. Chem Soc Rev 2017;46:4895–950.
[6] Blackman ML, Royzen M, Fox JM. Tetrazine ligation: fast bioconjugation based on inverse-electron-demand Diels–Alder reactivity. J Am Chem Soc 2008;130:13518–9.
[7] Rossin R, Läppchen T, van den Bosch SM, Laforest R, and Robillard MS. Diels–Alder reaction for tumor pretargeting: in vivo chemistry can boost tumor radiation dose compared with directly labeled antibody. J Nucl Med 2013;54:1989.
[8] García-Vázquez R, Battisti UM, Herth MM. Recent advances in the development of tetrazine ligation tools for pretargeted nuclear imaging. Pharmaceuticals 2022;15:685.
[9] Rossin R, Renart Verkerk P, van den Bosch SM, Vulders RCM, Verel I, Lub J, et al. In vivo chemistry for pretargeted tumor imaging in live mice. Angew Chem Int Ed 2010;49:3375–8.
[10] Lewis MR, Wang M, Axworthy DB, Theodore LJ, Mallet RW, Fritzberg AR, et al. In vivo evaluation of pretargeted ^{64}Cu for tumor imaging and therapy. J Nucl Med 2003;44:1284.
[11] Zeglis BM, Sevak KK, Reiner T, Mohindra P, Carlin SD, Zanzonico P, et al. A pretargeted PET imaging strategy based on bioorthogonal Diels–Alder click chemistry. J Nucl Med 2013;54:1389.
[12] Evans HL, Nguyen Q-D, Carroll LS, Kaliszczak M, Twyman FJ, Spivey AC, et al. A bioorthogonal ^{68}Ga-labelling strategy for rapid in vivo imaging. Chem Commun 2014;50:9557–60.
[13] Meyer J-P, Kozlowski P, Jackson J, Cunanan KM, Adumeau P, Dilling TR, et al. Exploring structural parameters for pretargeting radioligand optimization. J Med Chem 2017;60:8201–17.
[14] Li Z, Cai H, Hassink M, Blackman ML, Brown RCD, Conti PS, et al. Tetrazine–trans-cyclooctene ligation for the rapid construction of ^{18}F labeled probes. Chem Commun 2010;46:8043–5.
[15] Liu G. A revisit to the pretargeting concept—a target conversion. Front Pharmacol 2018;9.
[16] Keinänen O, Fung K, Pourat J, Jallinoja V, Vivier D, Pillarsetty NK, et al. Pretargeting of internalizing trastuzumab and cetuximab with a ^{18}F-tetrazine tracer in xenograft models. EJNMMI Res 2017;7:95.
[17] Denk C, Svatunek D, Mairinger S, Stanek J, Filip T, Matscheko D, et al. Design, synthesis, and evaluation of a low-molecular-weight ^{11}C-labeled tetrazine for pretargeted PET imaging applying bioorthogonal in vivo click chemistry. Bioconjug Chem 2016;27:1707–12.

[18] García-Vázquez R, Battisti UM, Shalgunov V, Schäfer G, Barz M, Herth MM. [^{11}C]carboxylated tetrazines for facile labeling of trans-cyclooctene-functionalized peptobrushes. Macromol Rapid Commun 2022;43:2100655.
[19] Albu SA, Al-Karmi SA, Vito A, Dzandzi JPK, Zlitni A, Beckford-Vera D, et al. ^{125}I-tetrazines and inverse-electron-demand Diels–Alder chemistry: a convenient radioiodination strategy for biomolecule labeling, screening, and biodistribution studies. Bioconjug Chem 2016;27:207–16.
[20] Radjani Bidesi NS, Battisti UM, Lopes van de Broek S, Shalgunov V, Dall A-M, Bøggild Kristensen J, et al. Development of the first tritiated tetrazine: facilitating tritiation of proteins. ChemBioChem 2022;23:e202200539.
[21] Denk C, Wilkovitsch M, Aneheim E, Herth MM, Jensen H, Lindegren S, et al. Multifunctional clickable reagents for rapid bioorthogonal astatination and radio-crosslinking. ChemPlusChem 2019;84:775–8.
[22] Zhu J, Li S, Wängler C, Wängler B, Bruce Lennox R, Schirrmacher R. Synthesis of 3-chloro-6-((4-(di-tert-butyl[^{18}F]fluorosilyl)-benzyl)oxy)-1,2,4,5-tetrazine ([^{18}F]SiFA-OTz) for rapid tetrazine-based ^{18}F-radiolabeling. Chem Commun 2015;51:12415–8.
[23] Keinänen O, Li X-G, Chenna NK, Lumen D, Ott J, Molthoff CFM, et al. A new highly reactive and low lipophilicity fluorine-18 labeled tetrazine derivative for Pretargeted PET imaging. ACS Med Chem Lett 2016;7:62–6.
[24] Denk C, Svatunek D, Filip T, Wanek T, Lumpi D, Fröhlich J, et al. Development of a ^{18}F-labeled tetrazine with favorable pharmacokinetics for bioorthogonal PET imaging. Angew Chem Int Ed 2014;53:9655–9.
[25] Zheng Q, Xu H, Wang H, Du W-GH, Wang N, Xiong H, et al. Sulfur [^{18}F]fluoride exchange click chemistry enabled ultrafast late-stage radiosynthesis. J Am Chem Soc 2021;143:3753–63.
[26] Stéen EJL, Jørgensen JT, Denk C, Battisti UM, Nørregaard K, Edem PE, et al. Lipophilicity and click reactivity determine the performance of bioorthogonal tetrazine tools in pretargeted in vivo chemistry. ACS Pharmacol Transl Sci 2021;4:824–33.
[27] Otaru S, Paulus A, Imlimthan S, Kuurne I, Virtanen H, Liljenbäck H, et al. Development of [^{18}F]AmBF3 tetrazine for radiolabeling of peptides: preclinical evaluation and PET imaging of [^{18}F]AmBF3-PEG7-Tyr3-octreotide in an AR42J pancreatic carcinoma model. Bioconjug Chem 2022;33:1393–404.
[28] Otaru S, Niemikoski H, Sarparanta M, Airaksinen AJ. Metabolism of a bioorthogonal PET tracer candidate [^{19}F/^{18}F]SiFA-tetrazine in mouse liver microsomes: biotransformation pathways and defluorination investigated by UHPLC-HRMS. Mol Pharm 2020;17:3106–15.
[29] Cook BE, Archbold J, Nasr K, Girmay S, Goldstein SI, Li P, et al. Non-invasive imaging of antisense oligonucleotides in the brain via in vivo click chemistry. Mol Imaging Biol 2022;24:940–9.
[30] Bredack C, Edelmann MR, Borroni E, Gobbi LC, Honer M. Antibody-based in vivo imaging of central nervous system targets-;evaluation of a pretargeting approach utilizing a TCO-conjugated brain shuttle antibody and radiolabeled tetrazines. Pharmaceuticals 2022;15:1445.
[31] García-Vázquez R, Battisti UM, Jørgensen JT, Shalgunov V, Hvass L, Stares DL, et al. Direct Cu-mediated aromatic ^{18}F-labeling of highly reactive tetrazines for pretargeted bioorthogonal PET imaging. Chem Sci 2021;12:11668–75.
[32] Bratteby K, Shalgunov V, Battisti UM, Petersen IN, van den Broek SL, Ohlsson T, et al. Insights into elution of anion exchange cartridges: opening the path toward aliphatic ^{18}F-radiolabeling of base-sensitive tracers. ACS Pharmacol Transl Sci 2021;4:1556–66.
[33] Battisti UM, Bratteby K, Jørgensen JT, Hvass L, Shalgunov V, Mikula H, et al. Development of the first aliphatic ^{18}F-labeled tetrazine suitable for pretargeted PET imaging—expanding the bioorthogonal tool box. J Med Chem 2021;64:15297–312.
[34] Shalgunov V, Lopes van den Broek S, Vang Andersen I, García Vázquez R, Raval NR, Palner M, et al. Pretargeted imaging beyond the blood–brain barrier. RSC. Med Chem 2023;14:444–53.
[35] Herth MM, Ametamey S, Antuganov D, Bauman A, Berndt M, Brooks AF, et al. On the consensus nomenclature rules for radiopharmaceutical chemistry - reconsideration of radiochemical conversion. Nucl Med Biol 2021;93:19–21.
[36] Qu Y, Sauvage F-X, Clavier G, Miomandre F, Audebert P. Metal-free synthetic approach to 3-monosubstituted unsymmetrical 1,2,4,5-tetrazines useful for bioorthogonal reactions. Angew Chem Int Ed 2018;57:12057–61.
[37] Gupta M, Lee HJ, Barden CJ, Weaver DF. The blood–brain barrier (BBB) score. J Med Chem 2019;62:9824–36.
[38] Wager TT, Hou X, Verhoest PR, Villalobos A. Central nervous system multiparameter optimization desirability: application in drug discovery. ACS Chem Neurosci 2016;7:767–75.
[39] Battisti UM, García-Vázquez R, Svatunek D, Herrmann B, Löffler A, Mikula H, et al. Synergistic experimental and computational investigation of the bioorthogonal reactivity of substituted aryltetrazines. Bioconjug Chem 2022;33:608–24.
[40] Glaser M, Årstad E. “Click labeling” with 2-[^{18}F]fluoroethylazide for positron emission tomography. Bioconjug Chem 2007;18:989–93.
[41] Stéen EJL, Shalgunov V, Denk C, Mikula H, Kjær A, Kristensen JL, et al. Convenient entry to ^{18}F-labeled amines through the Staudinger reduction. Eur J Org Chem 2019;2019:1722–5.